NASA Technical Memorandum 102095

On the Applications of Algebraic Grid Generation Methods Based on Transfinite Interpolation

Hung Lee Nguyen
Lewis Research Center
Cleveland, Ohio

June 1989

NASA

ON THE APPLICATIONS OF ALGEBRAIC GRID GENERATION METHODS BASED ON TRANSFINITE INTERPOLATION

Hung Lee Nguyen
National Aeronautics and Space Administration
Lewis Research Center
Cleveland, Ohio 44135

E-4778

SUMMARY

Algebraic grid generation methods based on transfinite interpolation called the two-boundary and four-boundary methods are applied for generating grids with highly complex boundaries and yields grid point distributions that allow for accurate application to regions of sharp gradients in the physical domain or time-dependent problems with small length scale phenomena. Algebraic grids are derived using the two-boundary and four-boundary methods for applications in both two- and three-dimensional domains. Grids are developed for distinctly different geometrical problems and the two-boundary and four-boundary methods are demonstrated to be applicable to a wide class of geometries.

INTRODUCTION

Many different techniques have been developed for generating computational grids required in the finite difference or finite element solutions of partial differential equations on arbitrary regions. An emerging problem, however, is the generation of grid systems on which solutions can be obtained for complex boundary geometries. The importance of the choice of the grid is well known. A poorly chosen grid may cause results to be erroneous or may fail to reveal critical aspects of the true solution. Any partial differential equation (e.g., the Navier-Stokes equations) expressed in a Cartesian coordinate system can be transformed to a uniform grid in computational coordinate system, called the boundary-fitted coordinate system. The objective of the grid generation method is to provide the Jacobian matrix describing the transformation. Algebraic grid generation methods are highly advantageous for direct computation of the physical domain as a function of uniform computational grid. These methods generate boundary-fitted coordinate systems by algebraically defining distinct boundaries of the physical domain and interpolating between these boundaries (1) to (6). The algebraic boundary curves can be analytical function or numerical interpolating functions. These algebraic grid generation methods can generate boundary-fitted coordinate systems without the need to solve the partial differential equations. Precise control of the distribution of grid points in the physical spatial domain can be achieved by stretching functions (7) to (9). The Jacobian matrix of the transformation can be obtained rapidly and efficiently by direct analytical differentiation or by numerical differentiation. This is in contrast to the differential-equation grid generation method where a partial differential/system is numerically solved by iterative techniques for the mapping between the coordinate system of the physical spatial domain and the boundary-fitted coordinate system. The transformation matrix (the Jacobian matrix) must be obtained by numerical differentiation, and a grid change requires a new solution of the partial differential equation system (10) to (12). This approach can be very expensive for problems with three-dimensional

and time-dependent boundary-fitted coordinate systems. Once the boundary-fitted coordinate system has been generated by an algebraic or a differential-equation grid generation method, the set of governing equations, such as the Navier-Stokes equations, are transformed analytically via a generalized coordinate transformation. This results in a set of governing equations in which all derivatives are with respect to the boundary-fitted coordinates. For the finite-difference method of solution, the derivatives in the transformed governing equations are replaced by finite-difference formulas (13) to (15) to form the desired system of finite-difference equations.

Algebraic grid generation method based on transfinite interpolation called the two-boundary and four-boundary methods are used to generate grids for two and three-dimensional spatial domains with complex arbitrary geometries. A detailed description of the methods is presented in reference 1. These methods are highly versatile and have a wide variety of applications in both two and three dimensions. In the two-boundary method, two separate nonintersecting boundaries of the physical domain are defined by means of algebraic functions (or numerical interpolation functions). These functions have as independent variables, coordinates which are normalized to unity. The two boundaries that must be mapped correctly from the physical spatial domain/to the computational domain can have very complex shapes and can be two or three dimensions. The two-boundary method can map all of the boundaries of a physical spatial domain correctly if the two curved boundaries connect two straight lines (in the two-dimensional case) or flat surfaces (in the three-dimensional case).

Application of the two-boundary method based on transfinite interpolation for generating grid points involves the following seven major steps (refs. 1 and 2):

1. Define the nature of the coordinate transformation.

2. Select a time stretching function.

3. Select the two boundaries of the physical spatial domain that do not touch each other at any point and must be mapped correctly.

4. Describe the two boundaries selected in parametric form in coordinates of the transformed domain.

5. Define curves that connect the two boundaries by using transfinite interpolation.

6. Discretize the domain.

7. Control distribution of grid points by using stretching function.

The four-boundary method is used to algebraically generate grids for problems in which four boundaries of the spatial domain must be mapped correctly from the physical spatial domain to the computational domain to the computational domain. The four boundaries that must be mapped correctly can have complex shapes and can be two or three dimensions. The four-boundary method is an extension of the two-boundary method (ref. 1). The procedure for applying the four-boundary method is similar to the seven steps described earlier for the

two-boundary method. The four-boundary method involves mapping the four boundaries of the spatial domain correctly to the transformed computational domain.

In this investigation, the two-boundary method is applied to generate grid points for the two-dimensional step dump combustor, the two-dimensional venturi nozzle, the two-dimensional step dump combustor with wedge-shaped solid bodies embedded inside the physical spatial domain.

ALGEBRAIC GRID GENERATION FOR A STEP DUMP COMBUSTOR

The two-boundary method is applied to the two-dimensional axisymmetric step dump combustor. Figure 1 shows the physical spatial domain of the two dimensional axisymmetric dump combustor. Because of the symmetry of this problem, grid points are generated for only half of the dump combustor. The physical spatial domain consists of region A enclosed by curves 1, 2, 3 and 4 and region B enclosed by curves 5, 6, 7 and 8 as shown in figure 1. If the upper curves of the spatial domain shown in figure 1 are replaced by a single curve displaying a sudden step at location B, the spatial derivatives of this/curve forming the upper boundary of the domain will contain discontinuities at location B. Then the metric coefficients of the transformation needed to obtain solution to the conservation equation governing the problem will be discontinuous at grid points on the boundary at location B and this discontinuity on the boundary will propagate into the interior of the spatial domain. Therefore the spatial domain of interest is divided into regions A and B which are patched together across common boundaries as shown in figure 1. It is necessary to match the grids across the common boundaries and to maintain control over the grid spacing in these regions.

In the following, the seven steps of the two-boundary method are applied to generate grid points for the step dump combustor.

Step 1 - Define the Coordinate Transformation

Since the two-dimensional spatial domain shown in figure 1 is nondeforming and the grid points in the x-y-t coordinate system will not move, the mapping of grid points in regions A and B involves the following coordinate transformation:

Region A:

$$1 \leq \xi \leq IL$$

$$1 \leq \eta \leq JL1$$

$$(x_A, y_A, t) \rightleftharpoons (\xi, \eta, \tau) \tag{1}$$

where

$$t = t(\tau) \tag{2}$$

$$x_A = x_A(\xi, \eta) \tag{3}$$

$$y_A = y_A(\xi,\eta) \tag{4}$$

Region B:

$$IL1 \leq \xi \leq IL$$

$$JL1 \leq \eta \leq JL$$

$$(x_B, y_B, t) \rightleftharpoons (\xi, \eta, \tau) \tag{5}$$

where

$$t = t(\tau) \tag{6}$$

$$x_B = x_B(\xi,\eta) \tag{7}$$

$$y_B = y_B(\xi,\eta) \tag{8}$$

where x-y-t represents the coordinate system of the physical domain and represents a boundary-fitted coordinate system of the transformed domain (fig. 1).

Step 2 - Select a Time Stretching Function

Since there is no stretching in time for both regions A and B, the relationship between t and τ is to be taken

$$t = \tau \tag{9}$$

Step 3 - Select Two Boundaries for Each Region

For the spatial domain shown in figure 1, curves 1 and 2 in region A are chosen to correspond to coordinate lines $\eta = 1$ and $\eta = JL1$, respectively. Curves 5 and 6 are chosen to correspond to $\eta = JL1$ and $\eta = JL$, respectively (fig. 1), i.e.,

Region A:

$$X_1 = x(\xi, \eta = 1) = X_1(\xi) \tag{10}$$

$$Y_1 = y(\xi, \eta = 1) = Y_1(\xi) \tag{11}$$

$$X_2 = x(\xi, \eta = JL1) = X_2(\xi) \tag{12}$$

$$Y_2 = y(\xi, \eta = JL1) = Y_2(\xi) \tag{13}$$

Region B:

$$X_5 = x(\xi, \eta = JL1) = X_5(\xi) \tag{14}$$

$$Y_5 = y(\xi, \eta = JL1) = T_5(\xi) \tag{15}$$

$$X_6 = x(\xi, n = JL) = X_6(\xi) \tag{16}$$

$$Y_6 = y(\xi, n = JL) = Y_6(\xi) \tag{17}$$

The two boundary method can map all of the boundaries of the physical domain correctly if the remaining boundaries are straight lines as in the present problem. As will be shown in step 4, the remaining boundaries, curves 2, 4 of region A and curves 7, 8 of region B, are mapped to coordinate lines $\xi = 1$, $\xi = IL$ and $\xi = IL1$ and $\xi = IL$, respectively.

Step 4 - Define the Two Boundaries Selected in Parametric Form

Once the two boundaries have been chosen, the next problem is the representation of these two boundary functions in parametric form in terms of the parametric variable ξ. Note that since boundary lines 3 and 4 are mapped to coordinate line $\xi = 1$ and $\xi = IL$, respectively, the variable can only vary between 1 and IL (note that x varies between A and C, see fig. 1).

One approach is to choose the parametric variable ξ such that

$$\xi = \frac{X - X_{min}}{X_{max} - X_{min}} \qquad \xi_{min} \leq \xi \leq \xi_{max} \tag{18}$$

By substituting equation (18) into equations (10) to (17), the desired parametric equations are obtained.

Region A:

$$X_1(\xi) = X_2(\xi) = (B - A)\xi + A, \qquad 1 \leq \xi = \frac{x - A}{B - A} \leq IL1 \tag{19}$$

$$X_1(\xi) = X_2(\xi) = (C - B)\xi + B, \qquad IL1 \leq \xi = \frac{x - B}{C - B} \leq IL \tag{20}$$

$$Y_1(\xi) = D, \qquad 1 \leq \xi \leq IL \tag{21}$$

$$Y_2(\xi) = E, \qquad 1 \leq \xi \leq IL \tag{22}$$

Region B:

$$X_5(\xi) = (C - B)\xi + B, \qquad IL1 \leq \xi = \frac{x - B}{C - B} \leq IL \tag{23}$$

$$Y_5(\xi) = E \tag{24}$$

$$X_6(\xi) = (C - B)\xi + B, \qquad IL1 \leq \xi = \frac{x - B}{C - B} \leq IL \tag{25}$$

$$Y_6(\xi) = E + a \tag{26}$$

where A, B, C, D, E, and a are constants defined in figure 1.

Step 5 - Define Curves That Connect the Two Boundaries

By using transfinite interpolation based on Hermite interpolation to interpolate between the boundaries selected in step 3, (i.e., curves 1, 2 and curves 5, 6), the connecting curves can be readily obtained. Since the boundaries curves are themselves functions and can be determined independently, equations (3), (4) and (7), (8) can be rewritten as cubic polynomials.

Region A:

$$X_A(\xi,\eta) = X_1(\xi)h_1(\eta) + X_2(\xi)h_2(\eta) + \frac{\partial x(\xi,\eta = 1)}{\partial \eta} h_3(\eta) + \frac{\partial x(\xi,\eta = JL1)}{\partial \eta} h_4(\eta) \qquad (27)$$

$$Y_A(\xi,\eta) = Y_1(\xi)h_1(\eta) + Y_2(\xi)h_2(\eta) + \frac{\partial y(\xi,\eta = 1)}{\partial \eta} h_3(\eta) + \frac{\partial y(\xi,\eta = JL1)}{\partial \eta} h_4(\eta) \qquad (28)$$

Region B:

$$X_B(\xi,\eta) = X_5(\xi)h_5(\eta) + X_6(\xi)h_6(\eta) + \frac{\partial x(\xi,\eta = JL1)}{\partial \eta} h_7(\eta) + \frac{\partial x(\xi,\eta = JL)}{\partial \eta} h_8(\eta) \qquad (29)$$

$$Y_B(\xi,\eta) = Y_5(\xi)h_5(\eta) + Y_6(\xi)h_6(\eta) + \frac{\partial y(\xi,\eta = JL1)}{\partial \eta} h_7(\eta) + \frac{\partial y(\xi,\eta = JL)}{\partial \eta} h_8(\eta) \qquad (30)$$

where $x_a(\xi,\eta)$, $y_a(\xi,\eta)$, $x_B(\xi,\eta)$, and $y_B(\xi,\eta)$ are connecting curves: X_1, Y_1, X_2, Y_2, X_5, Y_5, X_6, and Y_6 are given by equations (19) to (26); $h_1(\eta)$, $h_2(\eta)$, $h_3(\eta)$, $h_4(\eta)$, $h_5(\eta)$, $h_6(\eta)$, $h_7(\eta)$, and $h_8(\eta)$ are the Hermite polynomials (ref. 3).

Applying a cubic connecting function implies that the physical grid can be forced to be orthogonal at the boundaries. In order for the connecting curves to connect curve 1 perpendicularly in the physical domain, the dot product of $\vec{e}_\xi$ (the vector tangent to curve 1) and $\vec{e}_\eta$ (the vector tangent to the connecting curve) at any point on curve 1 must be zero, i.e.,

$$\vec{e}_\xi \cdot \vec{e}_\eta = 0$$

or

$$\left[\frac{dX_1(\xi)}{d\xi}\vec{i} + \frac{dY_1(\xi)}{d\xi}\vec{j}\right]\left[\frac{\partial x(\xi,\eta = 1)}{\partial \eta}\vec{i} + \frac{\partial x(\xi,\eta = 1)}{\partial \eta}\vec{j}\right] = 0 \qquad (31)$$

$$\frac{dX_1}{d\xi}\frac{\partial x(\xi,\eta = 1)}{\partial \eta} + \frac{dY_1}{d\xi}\frac{\partial y(\xi,\eta = 1)}{\partial \eta} = 0 \qquad (32)$$

Applying this procedure will force the grid to be orthogonal at the boundary curve 1. Equation (32) gives the following two conditions:

$$\frac{\partial x(\xi,\eta = 1)}{\partial \eta} = -K_1(\xi)\,\frac{dY_1(\xi)}{d\xi} \tag{33}$$

$$\frac{\partial y(\xi,\eta = 1)}{\partial \eta} = +K_1(\xi)\,\frac{dX_1(\xi)}{d\xi} \tag{34}$$

Control of the orthogonality for the connecting functions at other boundaries 2, 5, and 6 is accomplished in a similar manner and yields the following conditions:

$$\frac{\partial x(\xi,\eta = JL1)}{\partial \eta} = -K_2(\xi)\,\frac{dY_2(\xi)}{d\xi} \tag{35}$$

$$\frac{\partial y(\xi,\eta = JL1)}{\partial \eta} = +K_2(\xi)\,\frac{dX_2(\xi)}{d\xi} \tag{36}$$

$$\frac{\partial x(\xi,\eta = JL1)}{\partial \eta} = -K_5(\xi)\,\frac{dY_5(\xi)}{d\xi} \tag{37}$$

$$\frac{\partial y(\xi,\eta = JL1)}{\partial \eta} = +K_5(\xi)\,\frac{dX_5(\xi)}{d\xi} \tag{38}$$

$$\frac{\partial x(\xi,\eta = JL)}{\partial \eta} = -K_6(\xi)\,\frac{dY_6(\xi)}{d\xi} \tag{39}$$

$$\frac{\partial y(\xi,\eta = JL)}{\partial \eta} = +K_6(\xi)\,\frac{dX_6(\xi)}{d\xi} \tag{40}$$

$K_1(\xi)$, $K_2(\xi)$, $K_5(\xi)$, and $K_6(\xi)$ can be related to the magnitude of the boundary curves and are chosen by trial and error to ensure the grid lines do not overlap each other at the interior of the physical domain. For the present problem

$$K_1(\xi) = K_2(\xi) = K_f[Y_2(\xi) - Y_1(\xi)] \tag{41}$$

$$K_5(\xi) = K_6(\xi) = K_f[Y_6(\xi) - Y_5(\xi)] \tag{42}$$

Substitution of equations (33) to (42) into equations (27), (28) and (29), (30) gives the desired connecting curves. Given the connecting curves and parametric boundary curves, a uniform computational grid can be mapped onto the physical domain forming a physical grid.

Step 6 - Discretize the Domain

The time domain in the ξ-η-τ coordinate system is discretized by replacing it with equally-incremented time levels, i.e.,

$$\tau^n = n\Delta\tau, \quad n = 0, 1, 2, \ldots \tag{43}$$

where τ^n denotes time at the n^{th} time level and $\Delta\tau$ is the time-step size.

The spatial domain in the ξ-η-τ coordinate system is discretized by replacing it with equally spaced grid points. The locations of the grid points are given by

Region A:

$$\xi_i = i, \quad i = 1, 2, \ldots, IL1, \ldots, IL \tag{44}$$

$$\eta_j = j, \quad j = 1, 2, \ldots, JL1, \ldots, JL \tag{45}$$

Region B:

$$\xi_i = i, \quad i = IL1, \ldots, IL \tag{46}$$

$$\eta_j = j, \quad j = JL1, \ldots, JL \tag{47}$$

Substitution of equations (44) and (45) into equations (27), (28) and equations (46) to (47) into equations (29), (30) gives the grid points in the physical spatial domain.

Step 7 - Control Distribution of Grid Points

The two-boundary method is applied to generate grids inside the step dump combustor. Boundary layer flow near the wall of the combustor is characterized by strong viscid-inviscid interactions; in addition, one expects/steep velocity gradients at the injector location upstream of the rearward-facing step region. Thus, more grid points should be clustered near curves 2, 5, 6, and 8 along $x = x_{inj}$. Concentration of grid points near curves 2, 5, 6 is accomplished by replacing η in equations (27) to (30) by the following equation

$$\frac{(B_\eta + 1) - (B_\eta - 1)[(B_\eta + 1)/(B_\eta - 1)]^{(1-\xi)}}{[(B_\eta + 1)/(B_\eta - 1)]^{(1-\xi)} + 1} \tag{48}$$

In the above equation, B_η is a constant greater than unity. To concentrate more grid points near curve 8, ξ in equations (29) and (30) is replaced by the following equation

$$\frac{(B_\eta + 1)[(B_\eta + 1)/(B_\eta - 1)]^{(2\xi-1)} - B_\eta + 1}{2\{1 + [(B_\eta + 1)/(B_\eta - 1)]^{(2\xi-1)}\}} \tag{49}$$

To concentrate grid points along $x = x_{inj}$, replace ξ in equations (27) and (28) by the following expression

$$\xi_{inj}\left\{\frac{\sinh[B_\xi(\xi - \alpha)]}{\sinh(\alpha B_\xi)} + 1\right\} \tag{50}$$

where

$$\alpha = \frac{1}{2B_\xi} \ln \left[\frac{1 + (e^{B_\xi} - 1)\xi_{inj}}{1 + (e^{-B_\xi} - 1)\xi_{inj}} \right]$$

In the above equations, B_ξ is a constant greater than zero. By varying the parameter B_η and B_ξ, is different distributions of grid points can be obtained next to curves 2, 5, and 6 and along curve 8 and $x = x_{inj}$.

Figure 2 shows grid points generated inside the axisymmetric step dump combustor with no stretching functions used and with 51 grid points spanning the ξ direction and 21 grid points spanning the η direction. The grid system shown in Figure 3 was generated by using stretching functions (7) to (9). Approximately 50 sec of the IBM 370 CPU time is required to generate the grid system shown in figure 2.

ALGEBRAIC GRID GENERATION FOR A VENTURI NOZZLE

The two-boundary method is applied to the axisymmetric venturi nozzle. Because of the symmetry of this problem, grid points are generated for only half of the nozzle. Figure 4 shows the physical domain of the nozzle geometry. By following step 1 to 7 described above, a system of grid points is generated in the physical spatial domain. The following set of parametric boundary equations are used (step 4)

$$X_1(\xi) = (C - A)\xi + A \tag{51}$$

$$Y_1(\xi) = D \tag{52}$$

$$X_2(\xi) = (C - A)\xi + A \tag{53}$$

$$Y_2(\xi) = (E + a_1) + a_1 \cos \frac{\pi[(C - A)\xi]}{B - A}, \qquad 1 \le \xi \le \frac{B - A}{C - A} \tag{54}$$

$$= (E + a_2) - a_2 \cos \frac{\pi(C - A)\xi]}{C - B}, \qquad \frac{B - A}{C - A} < \xi \le IL \tag{55}$$

$$\xi = \frac{x - A}{c - A}$$

where A, B, C, D, E, a_1, and a_2 are constants defined in figure 4.

Figure 5 shows grid points generated inside the axisymmetric nozzle with no stretching function used and with 51 points spanning the ξ direction and 21 grid points spanning the η direction. Approximately 50 sec of the IBM 370 CPU time is required to generate the grid system shown in figure 5. The non-uniformly distributed grid system shown in figure 6 was generated with the use of stretching function. Comparing figure 5 and 6 indicates that the stretching functions employed can cluster grid points near the wall of the nozzle.

$$\xi = \frac{x - A}{c - A}$$

ALGEBRAIC GRID GENERATION FOR A STEP DUMP COMBUSTOR WITH EMBEDDED SOLID BODIES

To evaluate the feasibility of the two-boundary method, a two-dimensional axisymmetric step dump combustor with geometrically-complex embedded solid bodies is considered. The flow field domain is divided into five subdomains as shown in figure 7, each covering only part of the whole field. Grid points are generated inside each of the subdomain using the two-boundary method. The grid systems of these subdomains are interfaced with each other in such a way that the grid lines are continuous at the common boundaries.

Figure 7 shows the physical domain of the step dump combustor geometry together with the partitioned subdomains. The two-boundary method is applied to each of regions A, B, C, D, and E. The boundary curves are defined as described below.

Region A:

$$IL4 \leq \xi \leq IL$$

$$1 \leq \eta \leq JL1$$

Curve 1:

$$X_1(\xi) = E + (F - E)\left(\frac{X - E}{F - E}\right) \tag{55}$$

$$Y_1(\xi) = P \tag{56}$$

Curve 2:

$$X_2(\xi) = E + (F - E)\left(\frac{X - E}{F - E}\right) \tag{57}$$

$$Y_2(\xi) = Q \tag{58}$$

Region B:

$$1 \leq \xi \leq IL$$

$$JL1 \leq \eta \leq JL2$$

Curve 5:

$$X_5(\xi) = A + (B - A)\left(\frac{x - A}{B - A}\right), \qquad 1 \leq \xi \leq IL1 \tag{59}$$

$$= B + (C - B)\left(\frac{x - B}{C - B}\right), \qquad IL1 \leq \xi \leq IL2 \tag{60}$$

$$= C + (D - C)\left(\frac{x - C}{D - C}\right), \qquad IL2 \leq \xi \leq IL3 \tag{61}$$

$$= D + (E - D)\left(\frac{X - D}{E - D}\right), \qquad IL3 \leq \xi \leq IL4 \tag{62}$$

$$= E + (F - E)\left(\frac{X - E}{F - E}\right), \qquad IL4 \leq \xi \leq IL \tag{63}$$

$$Y_5(\xi) = P, \qquad 1 \leq \xi \leq IL2 \tag{64}$$

$$= P + (Q - P)\left(\frac{X - C}{D - C}\right), \qquad IL2 \leq \xi \leq IL3 \tag{65}$$

$$= Q, \qquad IL3 \leq \xi \leq IL \tag{66}$$

Curve 6:

$$X_6(\xi) = X_5(\xi), \qquad 1 \leq \xi \leq IL1 \tag{67}$$

$$= X_5(\xi), \qquad IL1 \leq \xi \leq IL2 \tag{68}$$

$$= X_5(\xi), \qquad IL2 \leq \xi \leq IL3 \tag{69}$$

$$= X_5(\xi), \qquad IL3 \leq \xi \leq IL4 \tag{70}$$

$$= X_5(\xi), \qquad IL4 \leq \xi \leq IL \tag{71}$$

$$Y_6(\xi) = S, \qquad 1 \leq \xi \leq IL2 \tag{72}$$

$$= S - (S - R)\left(\frac{X - C}{D - C}\right), \qquad IL2 \leq \xi \leq IL3 \tag{73}$$

$$= R, \qquad IL3 \leq \xi \leq IL \tag{74}$$

Region C:

$$IL4 \leq \xi \leq IL$$

$$JL2 \leq \eta \leq JL3$$

Curve 9:

$$X_9(\xi) = E + (F - E)\left(\frac{X - E}{F - E}\right) \tag{75}$$

$$Y_9(\xi) = E + (F - E)\left(\frac{X - E}{F - E}\right) \tag{76}$$

$$X_{10}(\xi) = X_9(\xi) \tag{77}$$

$$Y_{10}(\xi) = T \tag{78}$$

Region D:

$$1 \leq \xi \leq IL$$

$$JL3 \leq \eta \leq JL4$$

Curve 13:

$$X_{13}(\xi) = X_5(\xi), \qquad 1 \leq \xi \leq IL1 \tag{79}$$

$$= X_5(\xi), \qquad IL1 \leq \xi \leq IL2 \tag{80}$$

$$= X_5(\xi), \qquad IL2 \leq \xi \leq IL3 \tag{81}$$

$$= X_5(\xi), \qquad IL3 \leq \xi \leq IL4 \tag{82}$$

$$= X_5(\xi), \qquad IL4 \leq \xi \leq IL \tag{83}$$

$$Y_{13}(\xi) = S, \qquad 1 \leq \xi \leq IL2 \tag{84}$$

$$= S + (T - S)\left(\frac{X - C}{D - C}\right), \qquad IL2 \leq \xi \leq IL3 \tag{85}$$

$$= T, \qquad IL3 \leq \xi \leq IL \tag{86}$$

Curve 14:

$$X_{14}(\xi) = X_5(\xi), \qquad 1 \leq \xi \leq IL1 \tag{87}$$

$$= X_5(\xi), \qquad IL1 \leq \xi \leq IL2 \tag{88}$$

$$= X_5(\xi), \qquad IL2 \leq \xi \leq IL3 \tag{89}$$

$$= X_5(\xi), \qquad IL3 \leq \xi \leq IL4 \tag{90}$$

$$= X_5(\xi), \qquad IL4 \leq \xi \leq IL \tag{91}$$

$$Y_{14}(\xi) = U, \qquad 1 \leq \xi \leq IL2 \tag{92}$$

Region E:

$$IL1 \leq \xi \leq IL$$

$$JL4 \eta \leq JL$$

Curve 17:

$$X_{17}(\xi) = X_5(\xi), \qquad 1 \leq \xi \leq IL2 \tag{93}$$

$$= X_5(\xi), \qquad IL2 \le \xi \le IL3 \tag{94}$$

$$= X_5(\xi), \qquad IL3 \le \xi \le IL4 \tag{95}$$

$$= X_5(\xi), \qquad IL4 \le \xi \le IL \tag{96}$$

$$Y_{17}(\xi) = U, \qquad IL1 \le \xi \le IL \tag{97}$$

Curve 18:

$$X_{18}(\xi) = X_5(\xi), \qquad 1 \le \xi \le IL2 \tag{98}$$

$$= X_5(\xi), \qquad IL2 \le \xi \le IL3 \tag{99}$$

$$= X_5(\xi), \qquad IL3 \le \xi \le IL4 \tag{100}$$

$$= X_5(\xi), \qquad IL4 \le \xi \le IL \tag{101}$$

$$Y_{18}(\xi) = V, \qquad IL1 \le \xi \le IL \tag{102}$$

where the constants appearing in the above equations are defined in figure 7. The functional form for the connecting curves can be readily obtained by using Hermite interpolation to interpolate between the two boundaries selected for each of the subdomain.

Region A:

$$X_A(\xi,\eta) = X_1(\xi)h_1(\eta) + X_2(\xi)h_2(\eta) + \frac{\partial x(\xi,\eta = 1)}{\partial \eta} h_3(\eta) + \frac{\partial x(\xi,\eta = JL1)}{\partial \eta} h_4(\eta) \tag{103}$$

$$Y_A(\xi,\eta) = Y_1(\xi)h_1(\eta) + Y_2(\xi)h_2(\eta) + \frac{\partial x(\xi,\eta = 1)}{\partial \eta} h_3(\eta) + \frac{\partial x(\xi,\eta = JL1)}{\partial \eta} h_4(\eta) \tag{104}$$

Region B:

$$X_B(\xi,\eta) = X_5(\xi)h_5(\eta) + X_6(\xi)h_6(\eta) + \frac{\partial x(\xi,\eta = JL1)}{\partial \eta} h_7(\eta) + \frac{\partial x(\xi,\eta = JL2)}{\partial \eta} h_8(\eta) \tag{105}$$

$$Y_B(\xi,\eta) = Y_5(\xi)h_5(\eta) + X_6(\xi)h_6(\eta) + \frac{\partial x(\xi,\eta = JL1)}{\partial \eta} h_7(\eta) + \frac{\partial x(\xi,\eta = JL2)}{\partial \eta} h_8(\eta) \tag{106}$$

Region C:

$$X_C(\xi,\eta) = X_9(\xi)h_9(\eta) + X_{10}(\xi)h_{10}(\eta) + \frac{\partial x(\xi,\eta = JL2)}{\partial \eta} h_{11}(\eta) + \frac{\partial x(\xi,\eta = JL3)}{\partial \eta} h_{12}(\eta) \quad (107)$$

$$Y_C(\xi,\eta) = Y_9(\xi)h_9(\eta) + Y_{10}(\xi)h_{10}(\eta) + \frac{\partial x(\xi,\eta = JL2)}{\partial \eta} h_{11}(\eta) + \frac{\partial x(\xi,\eta = JL3)}{\partial \eta} h_{12}(\eta) \quad (108)$$

Region D:

$$X_D(\xi,\eta) = X_{13}(\xi)h_{13}(\eta) + X_{14}(\xi)h_{14}(\eta) + \frac{\partial x(\xi,\eta = JL3)}{\partial \eta} h_{15}(\eta) + \frac{\partial x(\xi,\eta = JL4)}{\partial \eta} h_{16}(\eta) \quad (109)$$

$$Y_D(\xi,\eta) = Y_{13}(\xi)h_{13}(\eta) + Y_{14}(\xi)h_{14}(\eta) + \frac{\partial x(\xi,\eta = JL3)}{\partial \eta} h_{15}(\eta) + \frac{\partial x(\xi,\eta = JL4)}{\partial \eta} h_{16}(\eta) \quad (110)$$

Region E:

$$X_E(\xi,\eta) = X_{17}(\xi)h_{17}(\eta) + X_{18}(\xi)h_{18}(\eta) + \frac{\partial x(\xi,\eta = JL4)}{\partial \eta} h_{19}(\eta) + \frac{\partial x(\xi,\eta = JL)}{\partial \eta} h_{20}(\eta) \quad (111)$$

$$Y_E(\xi,\eta) = Y_{17}(\xi)h_{17}(\eta) + Y_{18}(\xi)h_{18}(\eta) + \frac{\partial x(\xi,\eta = JL4)}{\partial \eta} h_{19}(\eta) + \frac{\partial x(\xi,\eta = JL)}{\partial \eta} h_{20}(\eta) \quad (112)$$

The Hermite polynominals are described previously derivative terms appearing in equations (103) to (112) are chosen so that the connecting curves perpendicularly intersect the boundaries selected above. Grid points inside this step dump combustor configuration are generated by using equations (103) to (112). Figure 8 shows grid points generated inside the spatial domain of this step dump cumbustor with 51 grid points spanning the ξ direction and 21 grid points spanning the η direction. Approximately 50 sec of the IBM CPU time is required to generate the grid system shown in figure 8. Figure 9 shows the grid system generated with the use of stretching functions.

ALGEBRAIC GRID GENERATION FOR A RECTANGULAR DUCT WITH ARBITRARY CROSS SECTIONS AND EMBEDDED SOLID BODIES

In this section, the four-boundary method (ref. 1) is applied to generate grid points for an axisymmetric rectangular duct with arbitrary cross sections and embedded solid bodies as shown in figure 10.

The grid is case in three dimensions by treating the three-dimensional spatial domain as a stack of two-dimensional spatial domains. The three-dimensional grid is generated by generating two-dimensional grids at equally incremented locations along the z-axis in the x-y-z-t coordinate system. Because of the symmetry of this problem, grid points are generated for only half of the duct shown in figure 10. The three-dimensional grid is obtained by rotating the upper half description about the axis of symmetry. Figure 11 shows the physical domain of the two-dimensional spatial domain. The spatial domain of interest is divided into regions A and B. The four-boundary method is applied to each of regions A and B by considering curves 1, 2, 3, and 4 as boundary curves of region A and curves 5, 6, 7, and 8 as boundary curves of region B.

The boundaries are defined as described below.

Region A:

$$1 \le \xi \le IL$$

$$1 \le \eta \le JL1$$

Curve 1:

$$x_1(\xi,\eta = 1) = X_1(\xi) = \left[\frac{\xi - 1}{IL - 1}(R_+ + R_-)\right] - R_- \tag{113}$$

$$y_1(\xi,\eta = 1) = Y_1(\xi) = R \tan \alpha_1 \tag{114}$$

Curve 2:

$$x_2(\xi,\eta = JL1) = X_2(\xi) = \left[\frac{\xi - 1}{IL - 1}(R_+ + R_-)\right] - R_- \tag{115}$$

$$y_2(\xi,\eta = JL1) = Y_2(\xi) = R \tan \alpha_2 \tag{116}$$

Curve 3:

$$x_3(\xi = 1,\eta) = X_3(\eta) = -R_- \tag{117}$$

$$y_2(\xi = 1,\eta) = Y_3(\eta) = \left[\frac{\eta - 1}{JL1 - 1}(R \tan \alpha_2 - R \tan \alpha_1)\right] + R \tan \alpha_1 \tag{118}$$

Curve 4:

$$x_4(\xi = IL,\eta) = X_4(\eta) = R_+ \tag{119}$$

$$y_4(\xi = IL,\eta) = Y_4(\eta) = \left[\frac{\eta - 1}{JL1 - 1}\,(R \tan \alpha_2 - R \tan \alpha_1)\right] + R \tan \alpha_1 \qquad (120)$$

Region B:

$$1 \le \xi \le IL$$

$$JL1 \le \eta \le JL$$

Curve 5:

$$x_5(\xi,\eta = JL1) = X_5(\xi) = \left[\frac{\xi - 1}{IL - 1}\,(R_+ + R_-)\right] - R_- \qquad (121)$$

$$y_5(\xi,\eta = JL1) = Y_5(\xi) = R \tan \alpha_3 \qquad (122)$$

Curve 6:

$$x_6(\xi,\eta = JL) = X_6(\xi) = \left[\frac{\xi - 1}{IL - 1}\,(R_+ + R_-)\right] - R_- \qquad (123)$$

$$y_6(\xi,\eta = JL) = Y_6(\xi) = R \tan \alpha_4 \qquad (124)$$

Curve 7:

$$x_7(\xi = 1,\eta) = X_7(\eta) = -R_- \qquad (125)$$

$$y_7(\xi = 1,\eta) = Y_7(\eta) = \left[\frac{\eta - JL1}{JL - JL1}\,(R \tan \alpha_4 - R \tan \alpha_3)\right] + R \tan \alpha_3 \qquad (126)$$

Curve 8:

$$x_8(\xi = IL,\eta) = X_8(\eta) = \left[\frac{\eta - JL1}{JL - JL1}\,(R \tan \alpha_4 - R \tan \alpha_3)\right] + R \tan \alpha_3 \qquad (127)$$

$$y_8(\xi = IL,\eta) = Y_8(\eta) = R \qquad (128)$$

where R, R_+, R_- α_1, α_2, α_3, and α_4 are defined in figure 11.

By using Hermite interpolation, cubic polynominals are used to generate connecting curves for the boundary curves. The connecting functions are

Region A:

$$X_A(\xi,\eta) = X^{(12)}(\xi,\eta) + X^{(34)}(\xi,\eta) - X^{(12)}(\xi = 1,\eta)h_5(\xi) - X^{(12)}(\xi = IL,\eta)h_6(\xi)$$

$$- \frac{\partial x^{(12)}(\xi = 1,\eta)}{\partial \xi}\,h_7(\xi) - \frac{\partial x^{(12)}(\xi = IL,\eta)}{\partial \xi}\,h_8(\xi) \qquad (129)$$

Region B:

$$Y_A(\xi,\eta) = Y^{(12)}(\xi,\eta) + Y^{(34)}(\xi,\eta) - Y^{(12)}(\xi = 1,\eta)h_5(\xi) - Y^{(12)}(\xi = IL,\eta)h_6(\xi)$$

$$- \frac{\partial y^{(12)}(\xi = 1,\eta)}{\partial \xi} h_7(\xi) - \frac{\partial x^{(12)}(\xi = IL,\eta)}{\partial \xi} h_8(\xi) \qquad (130)$$

where

$$X^{(12)}(\xi,\eta) = X_1(\xi)h_1(\eta) + X_2(\xi)h_2(\eta)$$

$$+ \frac{\partial x(\xi,\eta = 1)}{\partial \eta} h_3(\eta) + \frac{\partial x(\xi,\eta = JL1)}{\partial \xi} h_4(\eta) \qquad (131)$$

$$X^{(34)}(\xi,\eta) = X_3(\eta)h_5(\xi) + X_4(\eta)h_6(\xi)$$

$$+ \frac{\partial x(\xi = 1,\eta)}{\partial \xi} h_7(\xi) + \frac{\partial x(\xi = IL,\eta)}{\partial \xi} h_8(\xi) \qquad (132)$$

$$Y^{(12)}(\xi,\eta) = Y_1(\xi)h_1(\eta) + Y_2(\xi)h_2(\eta)$$

$$+ \frac{\partial y(\xi,\eta = 1)}{\partial \eta} h_3(\eta) + \frac{\partial y(\xi,\eta = JL1)}{\partial \eta} h_4(\eta) \qquad (133)$$

$$Y^{(34)}(\xi,\eta) = Y_3(\eta)h_5(\xi) + Y_4(\eta)h_6(\xi)$$

$$+ \frac{\partial y(\xi = 1,\eta)}{\partial \xi} h_7(\xi) + \frac{\partial y(\xi = IL,\eta)}{\partial \xi} h_8(\xi) \qquad (134)$$

$h_1(\xi)$, $h_2(\xi)$, $h_3(\xi)$, $h_4(\xi($, $h_5(\xi)$, $h_6(\xi)$, $h_7(\xi)$, and $h_8(\xi)$ are Hermite polynomials and are described previously.

The mapping between the physical domain and the transformed computational domain is obtained by using equations (113) to (134). Figure 12 shows the transformed domain in three dimension. Figure 10 shows grid points generated inside the axisymmetric rectangular duct with arbitrary cross section and solid bodies embedded in the interior physical domain with 41, 21, 31 grid points spanning the ξ, η, and ζ directions, respectively. Approximately 100 sec of the IBM 370 CPU time is required to generate the gird system shown in figure 10.

CONCLUSION

Algebraic grid generation method called the two-boundary method has been used to generate grid points inside the spatial domains of an axisymmetric step for dump combustor, an axisymmetric venturi nozzle and a step dump combustor with wedge-shaped solid bodies embedded inside the physical spatial domain.

Grids are generated for the three-dimensional rectangular duct with arbitrary cross sections and with solid bodies embedded inside the spatial domain using the four-boundary method. Grid generation for these complex arbitrary geometries can be obtained at a reasonably fast computer rate. The successful generation of grids for the cases studied demonstrates the usefulness and viability of the two-boundary and four-boundary algebraic grid generation methods.

REFERENCES

1. Shih, T.I-P.: Finite-Defference Methods in Computational Fluid Dynamics. To be published by Prentice Hall, Englewood Cliffs, NJ.

2. Thompson, J.F.; Warsi, Z.U.A.; and Mastin, C.W.: Boundary Fitted Coordinate Systems for Numerical Solution of Partial Differential Equations - A Review. J. Comput. Phys., vol. 37, July 1982, pp. 1-108.

3. Yang, S.-L.; and Shih, T.I-P.: An Algebraic Grid Generation Technique for Time-Varying Two-Dimensional Spatial Domains. Int. J. Numer. Meth. Fluids, vol. 6, May, 1986, pp. 291-304.

4. Thompson, J.F., ed.: Numerical Grid Generation. North Holland, 1982.

5. Smith, R.E.: Two-Boundary Grid Generation for the Solution of the Three-Dimensional Compressible Navier-Stokes Equations. NASA TM-83123, 1981.

6. Vinokur, M.; and Lombard, C.K.: Algebraic Grid Generation with Corner Singularities. Advances in Grid Generation, vol. 5, K.N. Ghia and Vrmila Ghia, eds., ASME, 1983, pp. 99-106.

7. Dolce, J.S.; Shih, T.I-P.; and Roan, V.P.: One-Dimensional Stretching Functions from a Variational Principle. CFDL Report No. 8801, Department of Mechanical Engineering, University of Florida, 1988.

8. Vinokur, M.: On One-Dimensional Stretching Functions for Finite-Difference Calculations. J. Comput. Phys., vol. 50, May, 1983, pp. 215-234.

9. Anderson, D.A.; Tannehill, J.C.; and Pletcher, R.H.: Computational Fluid Mechanics and Heat Transfer. Hemisphere Publishing Corp., Washington, 1984.

10. Mastin, C.W.; and Thompson, J.F.: Elliptic Systems and Numerical Transformations. J. Math. Anal. Appl., vol. 62, 1978, pp. 52-62.

11. Thompson, J.F.; Thames, F.C.; and Mastin, C.W.: Boundary-Fitted Curvilinear Coordinate Systems for Solution or Partial Differential Equations on Field Containing Any Number of Arbitrary Two-Dimensional Bodies. NASA CR-2729, 1977.

12. Thames, F.C., et al.: Numerical Solutions for Viscous and Potential Flow About Arbitrary Two-Dimensional Bodies Using Body-Fitted Coordinate Systems. J. Comput. Phys., vol. 24, July 1977, pp. 245-273.

13. Hirsh, R.S.: Higher Order Accurate Difference Solutions of Fluid Mechanics Problems by a Compact Differencing Technique. J. Comput. Phys., vol. 19, Sept. 1975, pp. 90-109.

14. Smith, G.D.: Numerical Solution of Partial Difference Equations: Finite Difference Methods. Second Ed., Clarendon Press, Oxford, 1978.

15. Steger, J.L.: Implicit Finite-Difference Simulation of Flow About Arbitrary Two-Dimensional Geometries. AIAA J., vol. 16, no. 7, July, 1978, pp. 679-686.

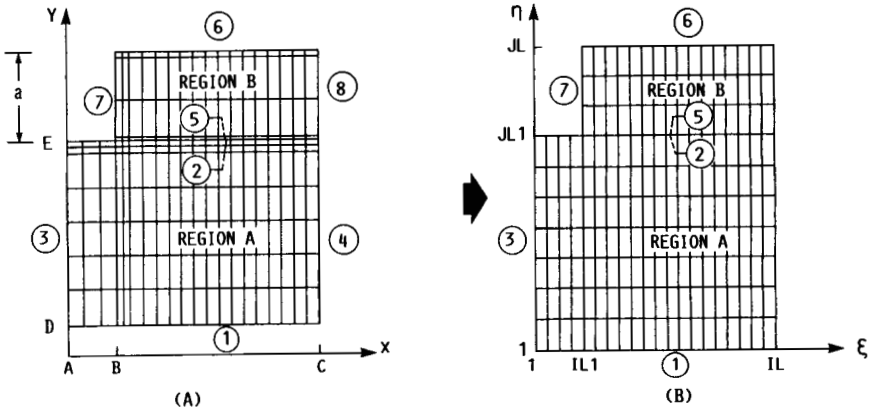

FIGURE 1. - (A) THE PHYSICAL SPATIAL DOMAIN. CURVE 1 IS DESCRIBED BY Y_1 = D WHEN x ∈ [A,C]. CURVE 2 IS DESCRIBED BY Y_2 = E WHEN x ∈ [A,C]. CURVE 5 IS DESCRIBED BY Y_5 = E WHEN X ∈ [B,C]. CURVE 6 IS DESCRIBED BY Y_6 = E + a WHEN x ∈ [B,C]. A, B, C, D, E, AND a ARE CONSTANTS. (B) TRANSFORMED COMPUTATIONAL DOMAIN.

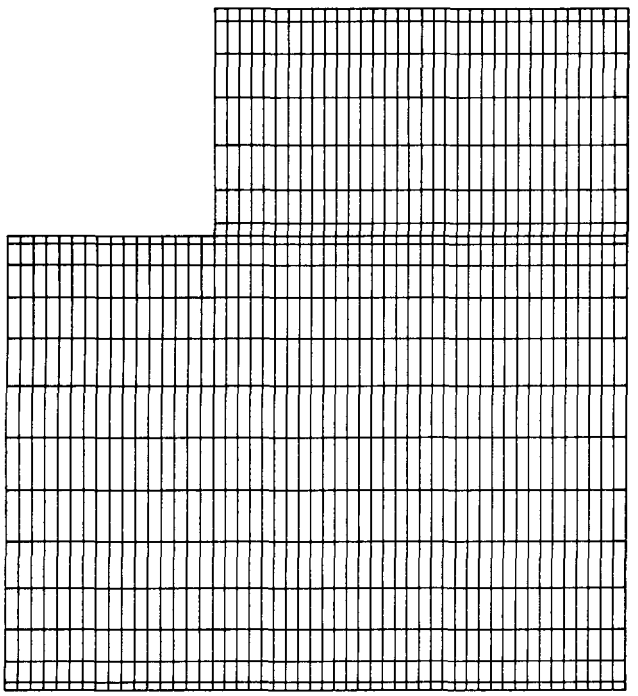

FIGURE 2. - GRID FOR STEP DUMP COMBUSTOR.

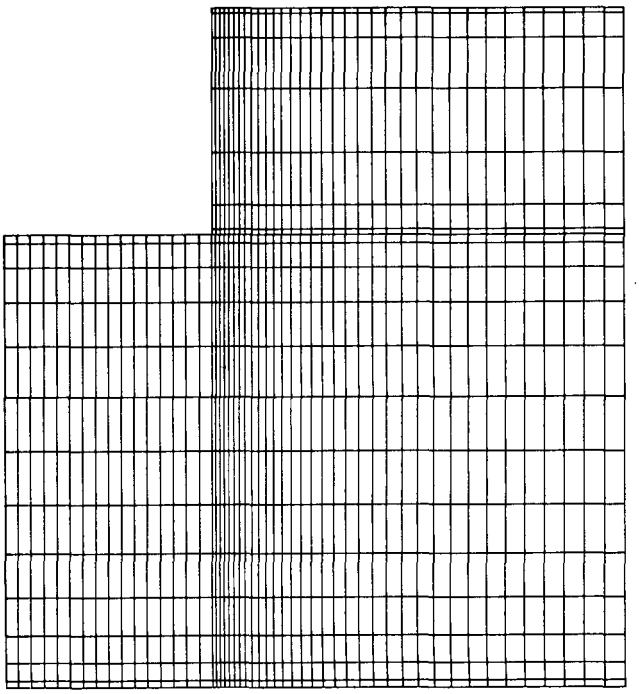

FIGURE 3. - GRID FOR STEP DUMP COMBUSTOR, STRETCHING FUNCTION USED.

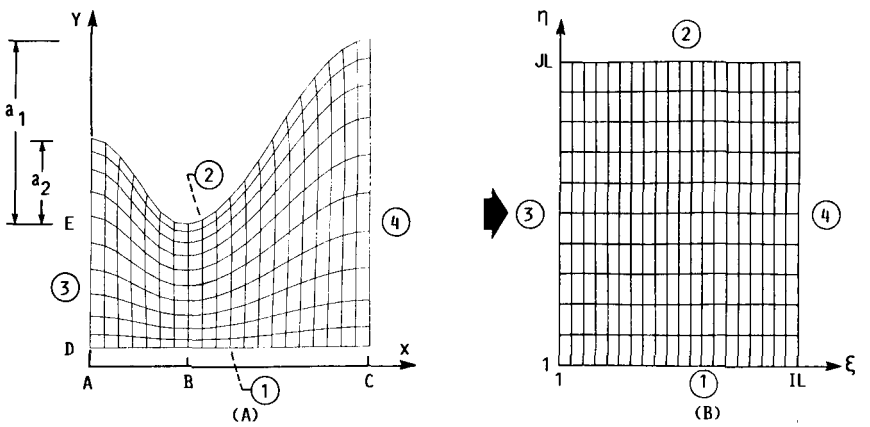

FIGURE 4. - (A) PHYSICAL SPATIAL DOMAIN. CURVE 1 IS DESCRIBED BY Y_1 = D WHEN x ε [A,C]. CURVE 2 IS DESCRIBED BY $Y_2 = (E + a_1) + a_1 \cos\left[\frac{\pi(x - A)}{B - A}\right]$ WHEN x ε [A,B] AND BY $Y_2 = (E + a_2) - a_2 \cos\left[\frac{\pi(x - B)}{C - B}\right]$ WHEN x ε [B,C]. A, B, C, D, E, a_1, AND a_2 ARE CONSTANTS. (B) TRANSFORMED COMPUTATIONAL DOMAIN.

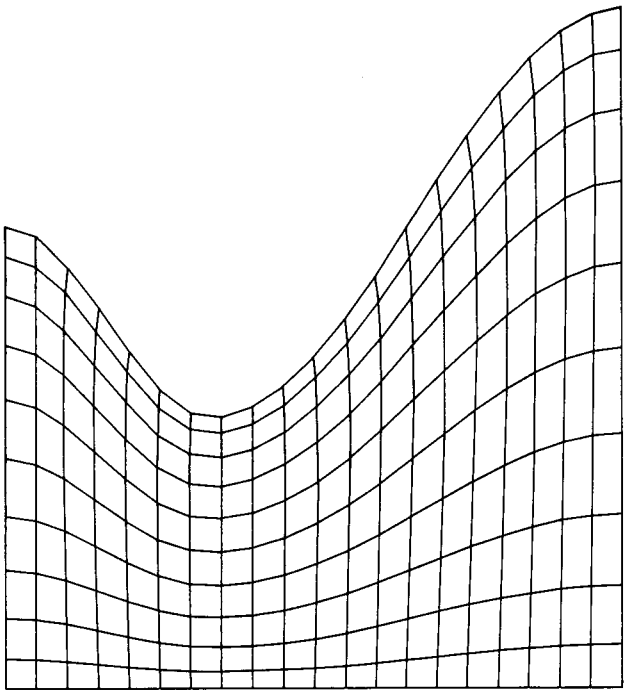

FIGURE 5. - GRID FOR VENTURIE NOZZLE.

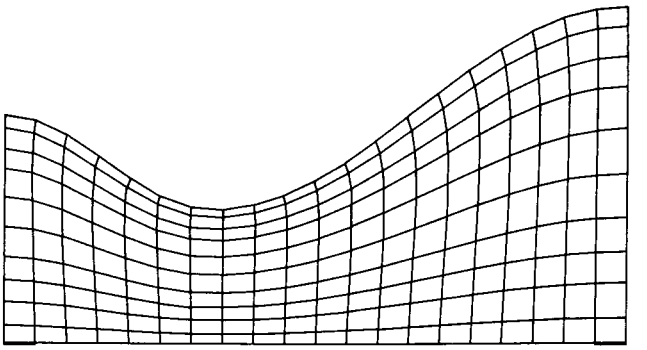

FIGURE 6. - GRID FOR VENTURIE NOZZLE, STRETCHING FUNCTION USED.

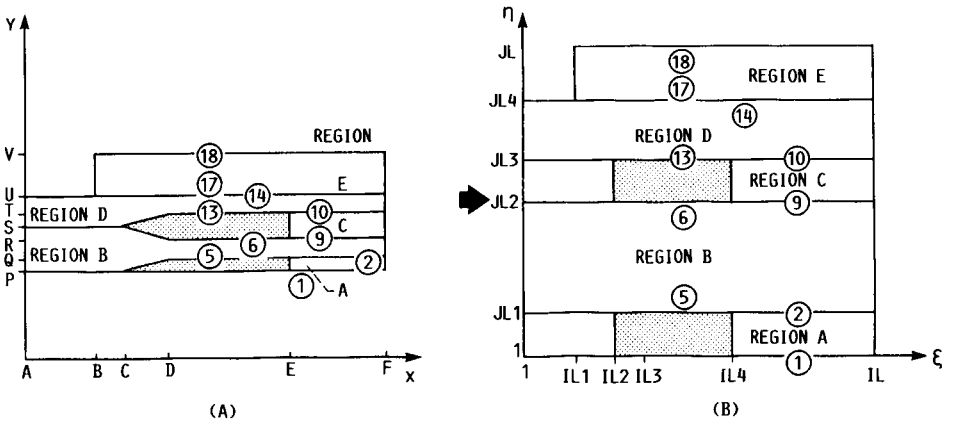

FIGURE 7. - (A) PHYSICAL SPATIAL DOMAIN. (B) TRANSFORMED COMPUTATIONAL DOMAIN.

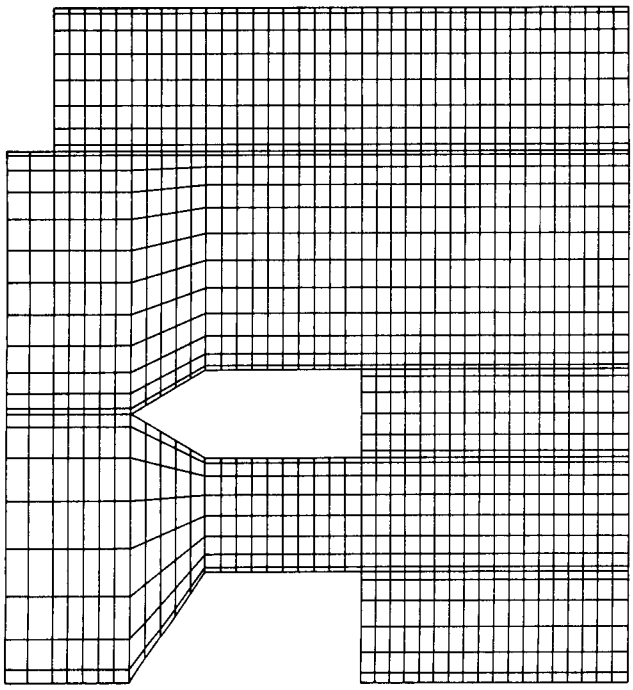

FIGURE 8. - GRID FOR STEP DUMP COMBUSTOR WITH EMBEDDED SOLID BODIES.

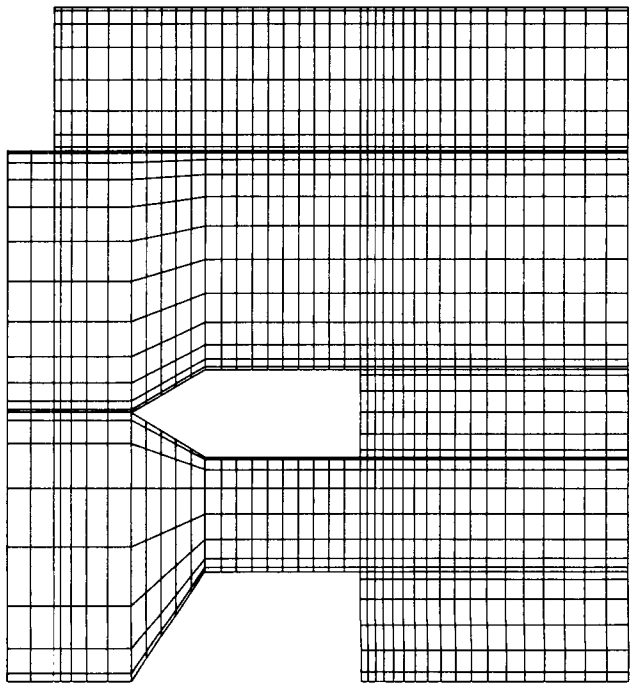

FIGURE 9. - GRID FOR STEP DUMP COMBUSTOR WITH EMBEDDED SOLID BODIES, STRETCHING FUNCTION USED.

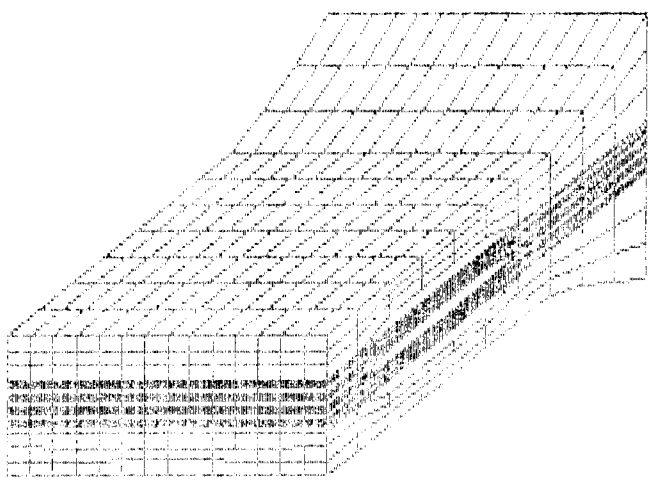

FIGURE 10. - GRID FOR RECTANGULAR DUCT GEOMETRY WITH EMBEDDED SOLID BODIES.

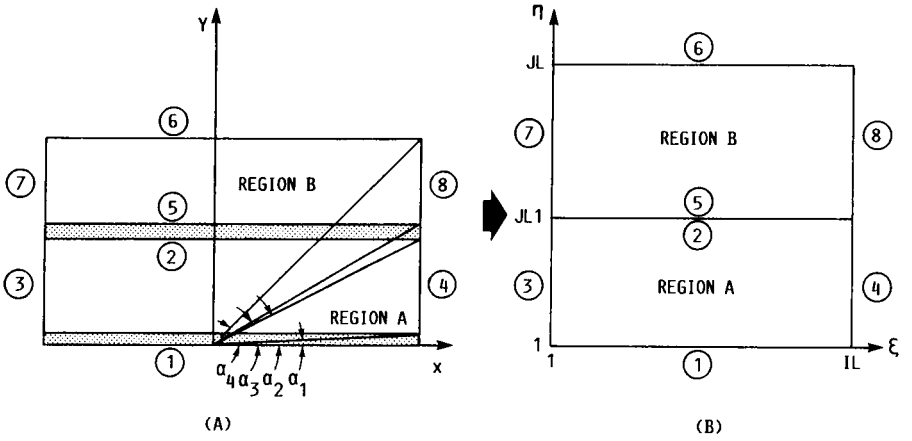

FIGURE 11. - (A) TWO-DIMENSIONAL PHYSICAL SPATIAL DOMAIN. (B) TWO-DIMENSIONAL COMPUTATIONAL DOMAIN.

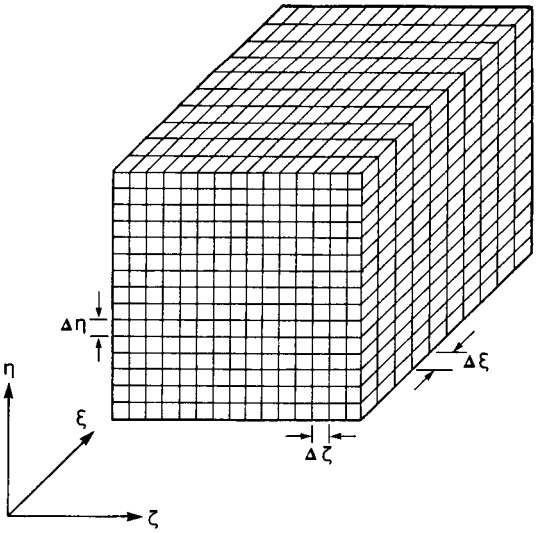

FIGURE 12. - THREE-DIMENSIONAL TRANSFORMED COMPUTATIONAL DOMAIN.

NASA
National Aeronautics and Space Administration

Report Documentation Page

1. Report No.	2. Government Accession No.	3. Recipient's Catalog No.
NASA TM-102095		

4. Title and Subtitle	5. Report Date
On the Applications of Algebraic Grid Generation Methods Based on Transfinite Interpolation	June 1989
	6. Performing Organization Code

7. Author(s)	8. Performing Organization Report No.
Hung Lee Nguyen	E-4778
	10. Work Unit No.
	505-62-61

9. Performing Organization Name and Address	11. Contract or Grant No.
National Aeronautics and Space Administration Lewis Research Center Cleveland, Ohio 44135-3191	
	13. Type of Report and Period Covered
	Technical Memorandum

12. Sponsoring Agency Name and Address	14. Sponsoring Agency Code
National Aeronautics and Space Administration Washington, D.C. 20546-0001	

15. Supplementary Notes

16. Abstract

Algebraic grid generation methods based on transfinite interpolation called the two-boundary and four-boundary methods are applied for generating grids with highly complex boundaries and yields grid point distributions that allow for accurate application to regions of sharp gradients in the physical domain or time-dependent problems with small length scale phenomena. Algebraic grids are derived using the two-boundary and four-boundary methods for applications in both two- and three-dimensional domains. Grids are developed for distinctly different geometrical problems and the two-boundary and four-boundary methods are demonstrated to be applicable to a wide class of geometries.

17. Key Words (Suggested by Author(s))	18. Distribution Statement
Algebraic grid generation; Two-boundary method; Four-boundary method; Two-dimensional grids; Three-dimensional grids	Unclassified – Unlimited Subject Category 07

19. Security Classif. (of this report)	20. Security Classif. (of this page)	21. No of pages	22. Price*
Unclassified	Unclassified	24	A03

*For sale by the National Technical Information Service, Springfield, Virginia 22161